

Field-reversed bubble in deep plasma channels for high quality electron acceleration

A. Pukhov¹, O. Jansen¹, T. Tueckmantel¹, J. Thomas¹ and I. Yu. Kostyukov^{2,3}

¹*Institut fuer Theoretische Physik I, Universitaet Duesseldorf, 40225 Germany*

²*Lobachevsky National Research University of Nizhny Novgorod, 603950, Nizhny Novgorod, Russia and*

³*Institute of Applied Physics RAS, Nizhny Novgorod 603950, Russia*

We study hollow plasma channels with smooth boundaries for laser-driven electron acceleration in the bubble regime. Contrary to the uniform plasma case, the laser forms no optical shock and no etching at the front. This increases the effective bubble phase velocity and energy gain. The longitudinal field has a plateau that allows for mono-energetic acceleration. We observe as low as 10^{-3} r.m.s. relative witness beam energy uncertainty in each cross-section and 0.3% total energy spread. By varying plasma density profile inside a deep channel, the bubble fields can be adjusted to balance the laser depletion and dephasing lengths. Bubble scaling laws for the deep channel are derived. Ultra-short pancake-like laser pulses lead to the highest energies of accelerated electrons per Joule of laser pulse energy.

PACS numbers: PACS1

The laser wake field acceleration (LWFA) [1] in underdense plasmas provides an option for high gradient particle acceleration [2]. Especially efficient is the *bubble regime* [3] when the laser expels background plasma electrons from the first half of the plasma wave. The advantage of the cavitated region is the transverse uniformity of its axial accelerating field [4] so that the energy gain of the accelerated electrons is not affected by their lateral motions in the bubble and the bunch can remain monoenergetic. The quasi-monoenergetic electron bunches are readily registered in experiments [5].

Despite various theoretical approaches: the phenomenological model of the bubble [4], the nonlinear theory of blowout regime [6, 7] and the similarity theory [8], - a self-consistent analytical description of the bubble regime is still absent.

The bubble theories exist for homogeneous plasmas only. Similarity theory together with energy conservation arguments resulted in the “optimal” scaling laws for homogeneous plasma [9]. These were tested in 3d PIC simulations [10]. The scalings assume that the laser energy is converted into the bubble fields first and then harvested by the electron bunch. The leading similarity parameters for the bubble in homogeneous plasmas are the S -number $S = n_e/an_c \ll 1$ and the pulse aspect ratio $\Pi = c\tau/R \leq 1$. Here, n_e is the plasma electron density and $n_c = \pi/r_e\lambda_0^2$ is the critical plasma density for a laser pulse with the wavelength λ_0 , $a = eE_0/mc\omega_0$ is the dimensionless laser amplitude, $\omega_0 = 2\pi c/\lambda_0$, and $r_e = e^2/mc^2$ is the classical electron radius, τ is the pulse duration and R is its radius.

In a uniform plasma, the bubble regime has some drawbacks. First, the laser energy depletion length is shorter than the electron dephasing length. This limits the maximum electron energy gain. Second, the transverse bubble fields acting on the accelerated electron bunch are strongly focusing. Thus, electrons running forward with the relativistic factor γ oscillate about the bub-

ble axis at the betatron frequency $\omega_\beta = \omega_p/\sqrt{2\gamma}$, where $\omega_p = \sqrt{4\pi e^2 n_e/m}$ is the background plasma frequency. A relativistic electron can easily come into betatron resonance with the Doppler-shifted laser that may result in energy exchange [11]. This betatron resonance broadens the electron bunch energy distribution and deteriorates the beam quality [12, 13].

Here, we consider the bubble regime of electron acceleration, but in a deep plasma channel rather than in a uniform plasma. This allows for a significant improvement of the acceleration. *We demonstrate that (i) the effective bubble phase velocity and energy gain increase in the channel; (ii) the longitudinal field has a plateau that allows for mono-energetic acceleration; (iii) the focusing force acting on the accelerated bunch is strongly reduced; (iv) the bubble scaling laws and the bubble field distribution for the deep channel are derived; (v) according to the new scaling laws, ultra-short pancake-like laser pulses match the dephasing and depletion length in the channel and thus lead to the highest energy gains of accelerated electrons per Joule of laser pulse energy.* In simulations, we observe as low as 10^{-3} r.m.s. relative witness beam energy uncertainty in each cross-section and 0.3% total energy spread. The lack of focusing in the channel eliminates the very possibility of a betatron resonance and leads to much sharper beam energy distributions.

Normally, plasma channels are used to guide weakly relativistic pulses over distances much larger than the Rayleigh length $Z_R = \pi R^2/\lambda_0$. These channels are shallow as a rule, i.e., the relative on-axis plasma density depletion is slight. Schroeder et al. [14] suggested recently the use of nearly hollow plasma channels to provide independent control over the focusing and accelerating forces. Chiou et al. [15] revealed that the transverse electric field of the wake is not monotonic in the hollow channel. However, these papers were limited only to a quasilinear regime of the plasma wake generation and a rectangular channel density profile.

W_L , J	2.2	17.6	141
τ , fs	4	8	16
R , μm	8	16	32
n_0 , $1/\text{cm}^3$	$5 \cdot 10^{18}$	$1.25 \cdot 10^{18}$	$0.31 \cdot 10^{18}$
R_{ch} , μm	6	12	24
l_i , μm	0.8	1.6	3.2
N_i , pC	10	20	40
\mathcal{E}_i , GeV	0.1	0.4	1.6
L_A , cm	1.6	12.8	100
$\mathcal{E}_{\text{max}}^{\text{dc}}$, GeV	1.5	6 (6)	23.5 (24)

Table I: Laser-plasma parameters used in the simulations and the observed electron energies. Expected energies from the scaling law are in brackets. All the lasers had $a_0 = 10$; the channel parameter $\delta = 0.3$.

A plasma channel is not required for laser guiding in the bubble regime, since the laser pulse is self-guided by the cavitated region of the bubble. Thus, a preformed shallow plasma channel is not expected to change the bubble dynamics significantly. However, as will be seen, a deep plasma channel i.e., one that is (nearly) empty on-axis, can strongly modify the bubble fields, the nonlinear laser dynamics, and the trapping. We are looking for laser-plasma parameters that maximize energy of the accelerated electron bunch and improve its quality: mainly, reduce the energy spread.

The laser pulse energy W_L is the technologically important characteristics of a laser pulse. It is limited, e.g. by size of the active crystal or by compression gratings, etc. We are comparing the energy scalings for the two cases: the uniform plasma case and the deep channel case.

In uniform plasma, the similarity scalings for electron bunch energy \mathcal{E}_{max} from a bubble [9] can be expressed in terms of the laser pulse power P_L , duration τ and energy $W_L = P_L \tau$:

$$\mathcal{E}_{\text{max}}^{\text{uniform}} \propto \sqrt{P_L e^2 c \tau} \lambda_0^{-1} = \lambda_0^{-1} \sqrt{W_L e^2 c \tau} \quad (1)$$

The scaling of Eq. (1) favors longer laser pulses. This reflects the mechanism of laser pulse depletion in the standard bubble. The laser pulse interacts with plasma electrons at the very front only. The major part of the pulse propagates freely in the cavitated region. Thus, the pulse tail slowly overtakes its head, where an ‘‘optical shock’’ is formed and the pulse ‘‘etches’’. This ‘‘etching’’ leads to the pulse shortening [16] and faster dephasing that in turn lowers the maximum energy gain. The highest electron energies are achieved with ‘‘spherical’’ laser pulses, whose duration $c\tau$ equals their radius R [10]. Such pulses fill the cavitated region completely and interact with the accelerated bunch affecting its quality.

Also, in the uniform plasma case, the bubble may continuously trap electrons causing strong beam loading and thus large energy spread. Also, the accelerating field

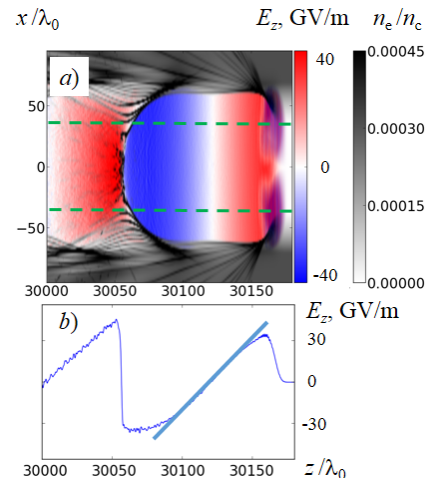


Figure 1: Simulation results for the case $R = 32 \mu\text{m}$. a) The cross-section of the plasma electron density and the longitudinal bubble field; b) on-axis accelerating field of the bubble, GV/m. Flattening of E_z at the bubble rear part is visible. The broken lines in frame (a) mark the vacuum part of the plasma channel. The purple rippling of the E_z at the bubble head is caused by the short laser pulse.

in the standard bubble is a linear function of the longitudinal coordinate [4, 6]. If one wants a truly monoenergetic acceleration of externally injected particles, the witness bunch to be accelerated must be extremely short. Demanding, e.g. 1% energy spread, the witness bunch should not occupy more than 1% of the bubble length.

The use of the deep plasma channel gives us several new control parameters to improve the acceleration. We consider channels with a zero plasma density on-axis and some smoothly growing density at the borders. We have chosen the following parameterization for the plasma radial profile: $n_e = n_0 [\delta \exp(r/R_{\text{ch}}) - 1]$, for $r \geq r_0$ and $n_e = 0$ for $r < r_0$, where $r_0 = R_{\text{ch}} \ln(1/\delta)$. Such profiles can be produced by ablation from walls of an empty capillary [17]. The parameters n_0 , δ , R_{ch} provide enough freedom to adjust fields in the channel while ensuring a smooth guiding of the relativistically intense laser pulse. In simulations, we reduced the maximum plasma density far from the channel axis for numerical stability.

The freedom on the bubble fields in the deep channel allows the achievement of much higher electron energies with a laser of a given pulse energy. Let us assume that the accelerating bubble field E is completely at our disposal and that the laser pulse energy is converted primarily into that field. The laser pulse energy scales as $W_L \propto R^2 I c \tau$, where I is the laser intensity. We omit dimensionless numerical factors like π etc. as we are interested in parametric dependencies only. The numerical pre-factors can be obtained from gauging the scaling laws against PIC simulations.

We can find the pulse depletion length L_d by com-

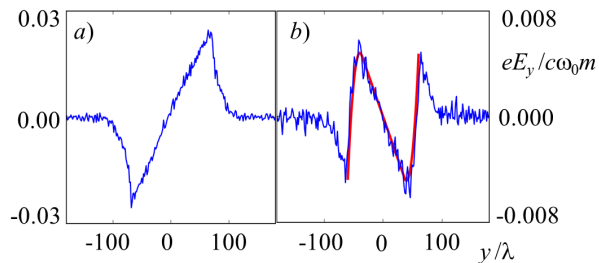


Figure 2: Transverse electric field of the bubble for the laser radius $R = 40\lambda_0$ and $a_0 = 10$. a) Homogeneous plasma: the field is focusing. b) Channel: the field reverses its sign in the channel walls; the smooth curve gives the analytic solution for the field E_y .

paring the energy deposited in the wake field $W_{\text{wake}} \propto E^2 R^2 L_d$ and the initial pulse energy, $W_{\text{wake}} = W_L$:

$$L_d \propto Ic\tau E^{-2}. \quad (2)$$

Here we assume a cylindrically symmetric bubble whose radius scales together with the laser radius R .

The particle acceleration is limited either by the laser pulse depletion (2), or by electron dephasing. In the uniform plasma case, it was the laser pulse depletion that limited acceleration in the bubble regime. In the deep channel case of interest here, however, the depletion length can be adjusted by properly choosing the accelerating field E , as can be seen from (2). The maximum particle energy is achieved when the depletion length L_d equals the dephasing length L_A . Otherwise, the maximum energy gain is limited by the shortest of the two lengths and is lower. The dephasing length scales as $L_A \propto R\gamma_L^2$, where γ_L is the relativistic γ -factor associated with the laser group velocity. In a deep plasma channel, γ_L is not influenced by the plasma and is defined solely by the laser pulse radius so that we can write $\gamma_L \propto k_0 R$, where $k_0 = 2\pi/\lambda_0$. For the dephasing length we obtain

$$L_A^{\text{dc}} \propto k_0^2 R^3 \quad (3)$$

We require the depletion length of Eq. (2) to be equal the dephasing length (3) and obtain for the bubble field $E \propto \sqrt{Ic\tau/k_0^2 R^3}$ in the deep plasma channel. This leads to the maximum energy gain scaling

$$\mathcal{E}_{\text{max}}^{\text{dc}} \propto eL_A E \propto e\sqrt{Ic\tau k_0^2 R^3} = k_0 \sqrt{mc^2 W_L r_e R} \quad (4)$$

The deep channel scaling (4) differs dramatically from the uniform plasma bubble scaling (1). While the uniform plasma case requires the maximum pulse duration τ , in

the deep channel, pulses with radius R as large as possible have an advantage.

A deeper insight in the bubble field configuration provides the quasistatic theory, which implies that the bubble slowly evolves in time and the bubble fields depend on $\xi = t - z$ [18–20]. The nonlinear theory of the bubble in homogeneous plasma [6] can be generalized to transversally inhomogeneous plasma (details be published elsewhere). It follows from the theory that the bubble field not too close to the edge of the bubble is defined by the source function $s(r_b) \equiv (1/2r_b^2) \int_0^{r_b} \rho_{\text{ion}}(r) r dr$:

$$\mathbf{E} \approx \mathbf{e}_r \left[\frac{2r_b^2 s(r)}{r} - rs(r_b) \right] - \mathbf{e}_z 2\xi s(r_b), \quad \mathbf{B} \approx -rs(r_b). \quad (5)$$

For homogeneous plasma $\rho_{\text{ion}}(r) = 1$ we recover known expression for the bubble field [4] $\mathbf{E} \approx \mathbf{e}_r r/4 - \mathbf{e}_z \xi/2$ and $\mathbf{B} \approx -e_\varphi r/4$. For the plasma channel with exponential profile discussed above the source function takes a form $s(r) = |e|n_0 (r_0^2 - r^2 + 2\eta r_{ch}\delta) / (4r_b^2)$, for $r \geq r_0$ and $s(r) = 0$ for $r < r_0$, where $\eta = \exp(r/r_{ch})(r - r_{ch}) + \exp(r_0/r_{ch})(r_{ch} - r_0)$. The obtained solution says that inside the vacuum part of the plasma channel $r < r_0$ the bubble field is purely electromagnetic $B_\varphi = E_r = 2(r/\xi)E_z$. In the channel walls, the ion field is added and can *reverse the sign of the transversal electric field* (see Fig.2). Another conclusion is that the plasma channel *reduces the gradients of the accelerating and focusing forces* in comparison with homogeneous plasma.

To check the quasi-static theory and the energy scalings, we perform a series of 3d PIC simulations using the code VLPL [21]. We run the code in laboratory frame for simulations with the smallest pulse radius. The laser pulse is circularly polarized and has the envelope $a(t, \mathbf{r}) = a_0 \exp(-r^2/R^2 - t^2/\tau^2)$. The envelope is cut to zero at $t = 2\tau$, $r = 2R$. We assume laser wavelength $\lambda_0 = 800$ nm.

We observe very little or no self-injection in the bubble when an empty on-axis channel is used. Thus, we inject an external co-propagating witness electron bunch at the end of the bubble. It has the half-length l_i , initial energy \mathcal{E}_i , and the total charge N_i . The simulation parameters are collected in Table I.

We selected an extremely short laser pulse with $\tau_0 = 4$ fs, $R_0 = 8 \mu\text{m}$, and energy of $W_L = 2.2$ J as the first member for the sequence of three in our power of 2 scaling sequence for both pulse duration and radius, as given in Table I. Although such short and energetic pulses do not exist yet, projects are under way to achieve similar parameters. According to the similarity rule, we scale simultaneously the laser pulse radius and duration with the same factor $\alpha = 2$ from stage n to stage $n + 1$: $R_{(n+1)} = \alpha R_{(n)}$ and $\tau_{(n+1)} = \alpha \tau_{(n)}$ so that the aspect ratio $\Pi = R/c\tau \approx 6.7$ remains fixed, i.e. the pulses are

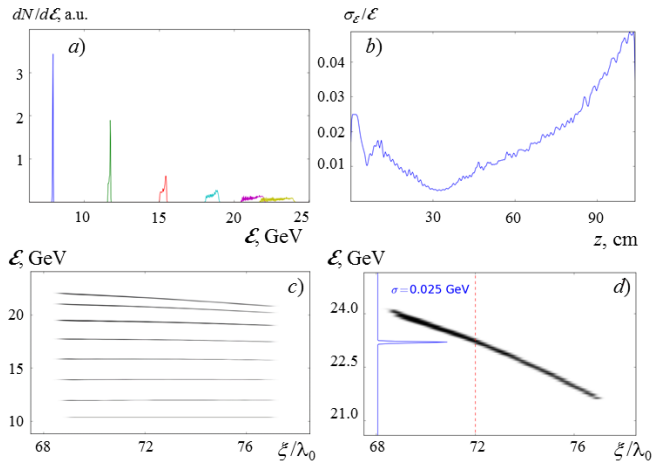


Figure 3: Simulation results for the case $R = 32 \mu\text{m}$ ($R = 40\lambda_0$). a) Energy spectra of the witness beam at different acceleration stages. b) Evolution of relative r.m.s. spectral width $\sigma_{\mathcal{E}_i}$. The homogeneous acceleration lasts for the first 30 cm and minimum spectral width of 0.3% is reached. Later, the bunch gains positive energy chirp due to dephasing and the spectrum widens. c) Longitudinal phase space of the witness bunch at different propagation distances. d) The final phase space of the bunch zoomed. The local energy uncertainty is 10^{-3} and is limited by numerical resolution.

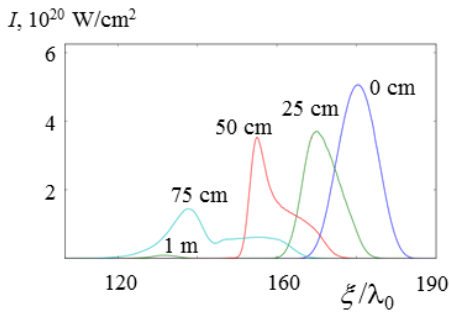


Figure 4: Nonlinear evolution of the laser pulse for the simulation case $R = 32 \mu\text{m}$. No typical for bubble regime pulse shortening or “optical shock” formation.

pancake-like. This allows us to reproduce the wake field (the bubble) *exactly* without additional search for the optimal plasma channel parameters. The other parameters scale as $R_{\text{ch}(n+1)} = \alpha R_{\text{ch}(n)}$, $n_{e(n+1)} = \alpha^{-2} n_{e(n)}$, $E_{(n+1)} = \alpha^{-1} E_{(n)}$, $L_{A(n+1)} = \alpha^3 L_{A(n)}$, and the particle energy scales as $\mathcal{E}_{\text{max}(n+1)} = \alpha^2 \mathcal{E}_{\text{max}(n)}$. The three scaled cases are digested in Table I. The most energetic pulse with $\tau_2 = 16$ fs, radius $R_2 = 32 \mu\text{m}$ and energy of $W_L = 141$ J would correspond to the planned Apollon laser [22]. The acceleration lengths range from $L_A = 2$ cm for the shortest laser, to $L_A = 1$ m for the largest laser pulse. These distances can be simulated only using the Lorentz boost [23].

The bubble generated by the largest laser pulse radius $R = 32 \mu\text{m}$ is shown in Fig.1. The accelerating field,

Fig.1(a), is transversely uniform. It allows for mono-energetic acceleration of wide electron bunches. This transverse field uniformity is also observed in homogeneous plasmas. The on-axis profile of the accelerating field in the channel, Fig.1(b), however, differs from that in the uniform plasma case. There is a region of flat accelerating field at the very back of the bubble. This region can be used to accelerate reasonably long witness bunches mono-energetically.

Fig.2 shows the bubble transverse fields in the bubble corresponding to the case $R = 40\lambda_0$ and $a_0 = 10$. We compare predictions of the quasi-static model with the numerical simulations. In the bubble center, $dE_y/dy \approx 0.08$, $dE_z/d\xi \approx 0.15 \approx 2(dE_y/dy)$ in the simulation and $dE_y/dy \approx 0.08$, $dE_z/d\xi \approx 0.16 = 2(dE_y/dy)$ in the models that is in a very good agreement. Fig.2(b) clearly shows the field reversal in the channel.

To check the acceleration, we inject a witness bunch that occupies about 10% of the bubble length. The energy spectra of the accelerated bunch are shown in Fig.3(a) at different times. The bunch stays very monoenergetic for the first 30 cm of acceleration, because it was injected in the flat accelerating field part of the bubble. The relative r.m.s. energy spread $\sigma_\epsilon/\mathcal{E}$, Fig.3(b), of the bunch is merely 0.3% when it gains 7.5 GeV energy. This is much better than the ratio of the bunch length to the bubble length that is 10%. Later, the bunch slowly leaves this flat E -field region and advances into the region with linearly growing E_z -field. Finally, it gains a positive energy chirp as seen in the bunch longitudinal phase space, Fig.3(c).

However, the quality of acceleration is best understood when we zoom in at the longitudinal phase space of the witness bunch, Fig.3(d). The r.m.s relative width of the witness bunch energy uncertainty taken at a particular longitudinal position is merely 10^{-3} and is probably defined by numerical resolution of our code. This very narrow energy spread is due to (i) the transverse uniformity of accelerating field in the bubble and (ii) the lack of a betatron resonance in the hollow channel.

Fig. 4 shows the nonlinear evolution of the laser pulse. Very different from the uniform plasma case, we observe no laser pulse shortening and no optical shock formation. The channel parameters were chosen to balance the dephasing length and the laser depletion length: $L_A = L_D = 1$ m.

In conclusion, we have shown that electron acceleration in deep plasma channels is scalable and the energy scalings favor ultra-short pancake-like laser pulses. The accelerating field has a nearly flat field region at the rear, where the accelerating field depends only slightly on the longitudinal coordinate. This allows for nearly monoenergetic acceleration of a witness bunch.

This work has been supported by the Deutsche Forschungsgemeinschaft via GRK 1203 and SFB TR 18, by EU FP7 project EUCARD-2 and by the Government

of the Russian Federation (Project No. 14.B25.31.0008) and by the Russian Foundation for Basic Research (Grants No. 13-02-00886, 13-02-97025).

-
- [1] E. Esarey, C. B. Schroeder, and W. P. Leemans, *Rev. Mod. Phys.* **81**, 1229 (2009)
- [2] C. Joshi and A. Caldwell, “Plasma Accelerators,” *Handbook for Elementary Particle Physics, Volume III*, edited by S. Myers and H. Schopper, Heidelberg, Springer (2013), 12-1.
- [3] A. Pukhov, J. Meyer-ter-Vehn, *Applied Physics B* **74**, 355 (2002)
- [4] I. Kostyukov, A. Pukhov, S. Kiselev, *Phys. Plasmas* **11**, 5256 (2004)
- [5] V. Malka *Laser Plasma Accelerators*, in *Laser-Plasma Interactions and Applications*, Scottish Graduate Series, pp 281-301 (2013)
- [6] W. Lu et al. *PRSTAB* **10**, 061301 (2007)
- [7] W. Lu et al., *Phys. Rev. Lett.* **96**, 165002 (2006).
- [8] S. Gordienko, A. Pukhov *Physics of Plasmas* **12**, 043109 (2004).
- [9] A. Pukhov, S. Gordienko, *Phil Tr. R. Soc. A*, **364**, 623 (2006).
- [10] O. Jansen, T. Tückmantel, and A. Pukhov, *Eur. Phys. J. Special Topics* **223**, 1017–1030 (2014)
- [11] A Pukhov, ZM Sheng, J Meyer-ter-Vehn, *Physics of Plasmas* **6**, 2847 (1999)
- [12] S. Cipiccia et al *Nature Physics* **7**, 867 (2011)
- [13] J L Shaw et al., arXiv:1404.4926 (2014)
- [14] C. B. Schroeder, E. Esarey, C. Benedetti, W. Leemans *Phys. Plasmas* **20**, 080701 (2013)
- [15] T. C. Chiou et. al., *Physics of Plasmas* **2**, 310 (1995)
- [16] J. Faure et al., *Phys. Rev. Lett.* **95**, 205003 (2005).
- [17] Y. Katzir et al. *Appl. Phys. Lett.* **95**, 031101 (2009).
- [18] P. Sprangle, E. Esarey, and A. Ting, *Phys. Rev. Lett.* **64**, 2011 (1990)
- [19] D. H. Whittum, *Phys. Plasmas*, **4**, 1154 (1997)
- [20] P. Mora and Th. M. Antonsen Jr., *Phys. Plasmas* **4**, (1997)
- [21] A. Pukhov *Journal of Plasma Physics* **61**, 425 (1999).
- [22] F. Giamb Bruno et al., *Appl. Opt.* **17**, 2617 (2011).
- [23] J.-L. Vay, C. G. R. Geddes, E. Cormier-Michel, and D. P. Grote, *Phys. Plasmas* **18**, 030701 (2011)